International Journal of Nanomedicine

Dovepress
open access to scientific and medical research

Open Access Full Text Article

ORIGINAL RESEARCH

EGFR-targeted delivery of DOX-loaded Fe_3O_4@ polydopamine multifunctional nanocomposites for MRI and antitumor chemo-photothermal therapy

This article was published in the following Dove Press journal:
International Journal of Nanomedicine
10 April 2017
Number of times this article has been viewed

Xupeng Mu[1]
Fuqiang Zhang[1]
Chenfei Kong[1]
Hongmei Zhang[1]
Wenjing Zhang[1]
Rui Ge[2]
Yi Liu[2]
Jinlan Jiang[1]

[1]Department of Central Laboratory, China-Japan Union Hospital, [2]State Key Laboratory of Supramolecular Structure and Materials, College of Chemistry, Jilin University, Changchun, China

Abstract: Multifunctional nanocomposites that have multiple therapeutic functions together with real-time imaging capabilities have attracted intensive concerns in the diagnosis and treatment of cancer. This study developed epidermal growth factor receptor (EGFR) antibody-directed polydopamine-coated Fe_3O_4 nanoparticles (Fe_3O_4@PDA NPs) for magnetic resonance imaging and antitumor chemo-photothermal therapy. The synthesized Fe_3O_4@PDA-PEG-EGFR-DOX NPs revealed high storage capacity for doxorubicin (DOX) and high photothermal conversion efficiency. The cell viability assay of Fe_3O_4@PDA-PEG-EGFR NPs indicated that Fe_3O_4@PDA-PEG-EGFR NPs had no cell cytotoxicity. However, Fe_3O_4@PDA-PEG-EGFR-DOX NPs could significantly decrease cell viability (~5% of remaining cell viability) because of both photothermal ablation and near-infrared light-triggered DOX release. Meanwhile, the EGFR-targeted Fe_3O_4@PDA-PEG-EGFR-DOX NPs significantly inhibited the growth of tumors, showing a prominent in vivo synergistic antitumor effect. This study demonstrated the potential of using Fe_3O_4@PDA NPs for combined cancer chemo-photothermal therapy with increased efficacy.

Keywords: Fe_3O_4 nanoparticles, polydopamine, chemo-photothermal therapy, multifunctional nanocomposites, DOX

Introduction

Recently, multifunctional nanocomposites that combine diagnostic and therapeutic functions have drawn an increasing concern. Ideally, in addition to safety and nontoxicity, these multifunctional nanocomposites should also have high drug-loading efficiencies and real-time imaging capabilities. More importantly, these nanocomposites should lead to lower toxicity to normal cells.[1,2] Magnetic Fe_3O_4 nanoparticles (NPs) is one of the inorganic-based nanomaterials approved for clinical use, which showed great biocompatibility and has attracted significant attention due to their unique characteristics such as magnetic resonance imaging (MRI) response to an external magnetic field.[3,4] Later, many biocompatible polymers, including chitosan, polyethylene glycol (PEG), and dextran, have been used to be coated in Fe_3O_4 NPs in order to further improve the properties of Fe_3O_4 NPs.[5–7]

As a major pigment of naturally occurring melanin,[8] polydopamine (PDA) is highly biocompatible and biodegradable.[9] Due to its nature, PDA has been widely used, to be coated in NPs, for various biomedical applications. Meanwhile, by dispersing the as-prepared cores in an alkaline dopamine solution, PDA could spontaneously form a conformal layer through in situ polymerization.[10] In addition, PDA has rich functional groups such as amino and catechol, which can facilitate the further functionalization

Correspondence: Jinlan Jiang
Department of Central Laboratory, China-Japan Union Hospital, Jilin University, 126 Xiantai Street, Changchun, 130033, China
Tel +86 431 8499 5432
Email jiangjinlan@jlu.edu.cn

submit your manuscript | www.dovepress.com
Dovepress
http://dx.doi.org/10.2147/IJN.S131418

of PDA-based NPs with biomolecules and can improve the stability and functionality of NPs.[9] Recent evidence has demonstrated that PDA-coated gold nanoshells could be stable within the cells of liver and spleen for at least 6 weeks.[10]

Photothermal therapy (PTT) is a new noninvasive cancer treatment technique, which is mediated by inorganic NPs responsive to near-infrared (NIR) light and could convert light energy into thermal energy.[11] As a new PTT agent, in addition to excellent biocompatibility in vitro and in vivo, PDA also had the strong NIR absorbance and high photothermal conversion efficiency (up to 40%).[12,13]

This study fabricated doxorubicin (DOX)-coated Fe_3O_4@PDA NPs that could be simultaneously used for NIR-response PTT, chemotherapy, and MRI. Although there were reports about the synthesis and applications of Fe_3O_4@PDA NPs,[14,15] to the best of our knowledge, the combination of PTT with chemotherapy (DOX) for the applications of antibody-targeted Fe_3O_4@PDA NPs has not been explored until now. Several reports showed that the tumors could not be completely eradicated by PTT alone due to the absorption and scattering of the NIR light by the biological tissues.[16,17] Then, integration of an efficient chemotherapy drug with PTT (termed chemo-photothermal therapy) is promising for enhanced and optimized antitumor efficacy.[18–20] DOX, as an aromatic chemotherapy drug, can be effectively loaded onto the PDA shell via π–π stacking. Using DOX-loaded NPs as the model system, it was confirmed that the intracellular uptake of Fe_3O_4@PDA-PEG-EGFR-DOX NPs and the release of DOX from Fe_3O_4@PDA-PEG-EGFR-DOX NPs localized inside the cells could be stimulated by NIR laser irradiation due to mild photothermal heating. The combined chemo-photothermal therapy achieved excellent synergistic therapeutic efficacy both in vitro and in vivo. The Fe_3O_4@PDA-PEG-EGFR NPs could further be utilized as the T_2 contrast agent in MRI to track tumor development. The results of the present study promised the use of Fe_3O_4@PDA core–shell NPs for combined antitumor chemo-photothermal therapy and MRI.

Materials and methods

Materials

Iron acetylacetonate (Fe (acac)$_3$), 1,2-hexadecanediol, benzyl ether, oleyamine (OLA), oleic acid (OA), sodium dodecyl sulfate (SDS), dopamine hydrochloride (DP), 1-ethyl-3-[3-dimethylaminopropyl] carbodiimide hydrochloride (EDC), and N-hydroxysuccinimide (NHS) were purchased from Millipore-Sigma (Darmstadt, Germany). Dulbecco's Modified Eagle's Medium (DMEM) with high glucose and fetal bovine serum (FBS) were purchased from Thermo Fisher Scientific (Waltham, MA, USA). NH_2-PEG-COOH (molecular weight =2,000 Da) was purchased from Seebio Biological (Shanghai, China). DOX hydrochloride was purchased from Sangon Ltd. (Shanghai, China). Anti-EGFR antibody was obtained from Ruiying Biological (Suzhou, China). Other reagents (analytical grade) were purchased from Beijing Chemical Reagents Company (Beijing, China) unless otherwise stated.

Cells and animals

The DLD-1 human colon cancer cell line was purchased from American Type Culture Collection (Manassas, VA, USA) and cultured in DMEM supplemented with 10% FBS in a humidified 5% CO_2 atmosphere at 37°C.

Female BALB/c nude mice (5–6 weeks old) were purchased from Vital River Company (Beijing, China) and were maintained under specific pathogen-free conditions. The animals were treated according to the ethical guidelines of Jilin University after obtaining approval from the Animal Welfare and Research Ethics Committee of Jilin University. The animal experiments were carried out following the internationally accepted animal care guidelines (EEC Directive of 1986; 86/609/EEC).

Preparation of Fe_3O_4@PDA-PEG-EGFR NPs

Fe_3O_4@PDA-PEG-EGFR NPs were prepared as shown in Figure 1. First, Fe_3O_4 NPs were synthesized as reported previously.[21] Second, to synthesize Fe_3O_4@PDA NPs, Tris-buffer (12 mL) was added into the as-prepared Fe_3O_4 NP solution and adjusted to pH 8.5, followed by adding different volumes of 0.03 M dopamine solution. The reaction mixture was incubated at room temperature for 3 h with the solution color gradually turning to dark brown, indicating in situ polymerization of dopamine. Last, the Fe_3O_4@PDA NPs were obtained by centrifugation at 10,000 rpm for 10 min and washed with deionized water.

Fe_3O_4@PDA-PEG NPs were synthesized as reported previously.[22] Briefly, for PEG modification, the as-prepared Fe_3O_4@PDA (10 mg) was reacted with NH_2-PEG-COOH (30 mg) in 50 mL Tris-buffer (0.01 M, pH 8.1) overnight under vigorous stirring. Then, PEGylated Fe_3O_4@PDA (termed Fe_3O_4@PDA-PEG) was purified by centrifugation at 10,000 rpm and redispersed in deionized water.

For EGFR antibody bioconjugation, EDC (5 mmoL) and NHS (12.5 mmoL) were dissolved in phosphate-buffered saline (PBS) containing Fe_3O_4@PDA-PEG NPs (pH 5.0). After 20 min, mouse anti-human EGFR monoclonal antibody

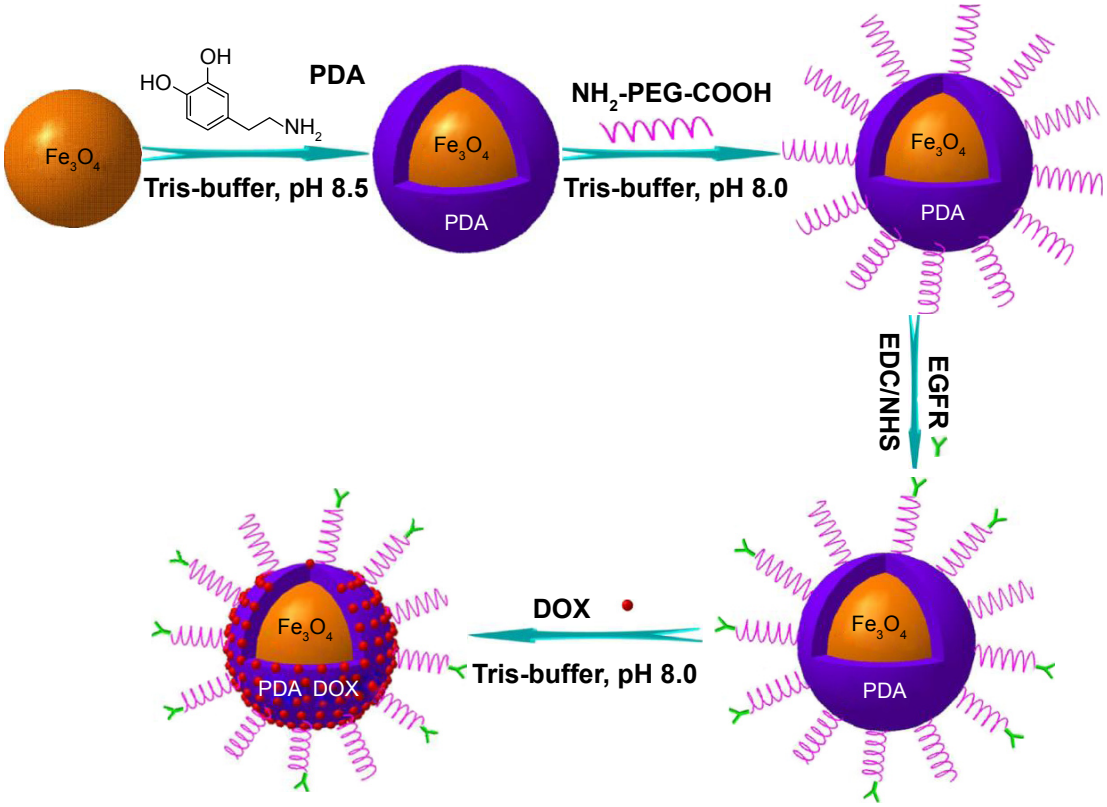

Figure 1 Schematic illustration of the synthesis and DOX loading of Fe_3O_4@PDA-PEG-EGFR NPs.
Abbreviations: DOX, doxorubicin; PDA, polydopamine; EDC, 1-ethyl-3-[3-dimethylaminopropyl] carbodiimide hydrochloride; NHS, N-hydroxysuccinimide; PEG, polyethylene glycol; NP, nanoparticle.

was added to this solution. Then, the pH of the reaction solution was adjusted to 7.5. The reaction lasted for 4 h at 4°C. The antibody-bioconjugated NPs (termed Fe_3O_4@PDA-PEG-EGFR NPs) were isolated by centrifugation and redispersed in deionized water.

Sodium dodecyl sulfate–polyacrylamide gel electrophoresis (SDS-PAGE)

The prepared Fe_3O_4@PDA-PEG-EGFR NPs were separated by a 10% SDS-PAGE according to the method of Laemmli.[23]

Immunofluorescence

DLD-1 cells were fixed in 4% paraformaldehyde for 15 min and permeabilized with 0.1% Triton X-100 in PBS for 30 min. Then, the cells were washed and blocked with 5% bovine serum albumin for 30 min. Cells were incubated with the primary EGFR antibodies (1:100; Ruiying Biological) overnight at 4°C. Then, the cells were washed and incubated with goat anti-mouse immunoglobulin G conjugated with fluorescein isothiocyanate for 1 h at room temperature. 4,6-Diamidino-2-phenylindole (DAPI; 1:10,000; Beyotime, Shanghai, China) was used for nucleus staining. Images were detected by using a fluorescence microscope (IX5-RFACA; Olympus Corporation, Tokyo, Japan).

Characterization of Fe_3O_4@PDA-PEG-EGFR NPs

The morphology of NPs was analyzed by using transmission electron microscope (TEM; Hitachi H-800 Hitachi, Tokyo, Japan). The size and its distribution of NPs were determined by dynamic light scattering (DLS) (Malvern Zetasizer Nano Instrument; Malvern Instruments, Malvern, UK). The zeta potentials of the as-prepared NPs were measured by using a Zetasizer Nano ZS (Malvern Instruments). The Fourier transform–infrared (FT-IR) spectroscopy of NPs was performed by using a Bruker Vertex 70 FT-IR spectrometer (Bruker, Karlsruhe, Germany) in the range from 400 to 4,000 cm^{-1}. A vibrating sample magnetometer was used for characterizing the magnetic properties of the NPs.

Loading DOX on Fe_3O_4@PDA-PEG-EGFR NPs

Fe_3O_4@PDA-PEG-EGFR NPs (1 mg) were suspended in 10× Tris-buffer (0.5 mL) and mixed with DOX solution (2 mL, 1 mg/mL). After 24 h of continuous stirring in the

dark, the obtained nanocomposites (named as Fe_3O_4@PDA-PEG-EGFR-DOX NPs) were purified by centrifugation and washed with deionized water. The loading weight of DOX was calculated as follows: $W = W_{original\ DOX} - W_{DOX\ in\ supernatant}$. The amount of DOX was determined by using the calibration curve of DOX at the wavelength of 480 nm.

pH- and photothermal-sensitive DOX release

Fe_3O_4@PDA-PEG-EGFR-DOX NPs were suspended in PBS at different pH, sealed in a dialysis bag (molecular weight cutoff =8,000 Da), and then were immersed into PBS solution at pH 5.0 or 7.4 at 37°C with moderate shaking for different periods of time. At desired time intervals, DOX in the release medium was collected, then the concentrations were determined by UV-vis spectrometry. The release medium was replaced with an equal volume of fresh PBS. The 808 nm NIR laser-triggered DOX release experiments were conducted following the same procedure as mentioned earlier. At predetermined time intervals, the samples were irradiated with an 808 nm NIR laser (0.6 W/cm^2) for 6 min. DOX in the dialysis buffer released from NPs was collected before and after 808 nm NIR laser irradiation.

In vitro photothermal experiments

A series of Fe_3O_4@PDA-PEG-EGFR NPs aqueous solutions with different concentrations (0, 25, 50, 75, 100, and 150 μg/mL) were irradiated with an 808 nm NIR laser (0.6 W/cm^2) for 6 min. The solution temperature was measured every 1 min by a thermometer with a thermocouple probe submerged in the solution. To detect the thermal stability of Fe_3O_4@PDA-PEG-EGFR NPs, the samples were irradiated for 6 min every time, followed by natural cooling of temperature to room temperature for five cycles, and the temperature was recorded every 1 min.

In vitro MRI of phantom

Fe_3O_4@PDA-PEG-EGFR NPs aqueous solutions with various concentrations (0, 15, 30, 60, 120, and 240 μg/mL) were prepared in 1.5 mL eppendorf tubes and swirled for 3 min before MRI. The T_2-weighted MRI was measured with a GE Sigma 3.0-T MR imaging system (General Electric, Milwaukee, WI, USA). The imaging parameters were listed as follows: TR, 1,390.0 ms; TE, 13.8 ms, field of view, 50×50 mm; and slice thickness, 2.5 mm.

Cellular uptake and internalization of Fe_3O_4@PDA-PEG-EGFR-DOX NPs

To study the cellular uptake and the intracellular distribution of Fe_3O_4@PDA-PEG-EGFR-DOX NPs, DLD-1 cells were incubated with Fe_3O_4@PDA-PEG-EGFR-DOX NPs (equal to DOX 5 μg/mL) for 6, 12, 24, and 36 h at 37.0°C. At predetermined time points after incubation, the cells were fixed with a 4% paraformaldehyde, and the cellular nuclei were stained with DAPI (1:10,000; Beyotime). The results were characterized by using a fluorescence microscope. In a separate experiment, DLD-1 cells were irradiated with the 808 nm NIR laser (0.6 W/cm^2) for 6 min after incubation with Fe_3O_4@PDA-PEG-EGFR-DOX NPs (equal to DOX 5 μg/mL) dispersions for 12 h. Then, the cells were treated in accordance with the aforementioned method and characterized by using a fluorescence microscope.

Cell viability assay

Cell Counting Kit-8 (CCK-8) assays were carried out to evaluate the potential cytotoxicity of Fe_3O_4@PDA-PEG-EGFR-DOX NPs. First, DLD-1 cells were seeded in a 96-well cell-culture plate at 200 μL (1×10^5 cells/mL) per well and incubated for 24 h. Then, the medium was removed, and the suspensions of Fe_3O_4@PDA-PEG-EGFR NPs or Fe_3O_4@PDA-PEG-EGFR-DOX NPs at selected concentrations (0, 6.25, 12.5, 25, 50, and 100 μg/mL) were added to the wells. The Fe_3O_4@PDA-PEG-EGFR NPs cells and Fe_3O_4@PDA-PEG-EGFR-DOX NPs-stained cells were irradiated by an 808 nm NIR laser (0.6 W/cm^2) for 6 min and were incubated at 37°C for another 24 h. Later, 10 μL of CCK-8 was added to each well. After incubation for 2 h, the absorbance of each well was read on a Microplate Reader (ELx-800; BioTek Instruments, Winooski, VT, USA) at 450 nm. The relative cell viability (%) related to the control wells containing cell-culture medium was calculated by using the following equation: Cell viability (%) = $A_{Test\ sample}/A_{Control} \times 100\%$, where $A_{Test\ sample}$ and $A_{Control}$ were the absorbance of the test sample and the control, respectively.

In vivo MRI

To develop the tumor model, DLD-1 cells (100 μL, 1×10^7/mL) suspended in PBS were inoculated subcutaneously into the back of each mouse. For in vivo MRI, desired amounts of Fe_3O_4@PDA-PEG-EGFR NPs in PBS solutions (100 μL) were injected intravenously into the mouse through the tail vein. In vivo MRI was performed at predetermined time points after injection. The T_2-weighted MRI parameters were shown as follows: TR, 3,980.0 ms; TE, 99.0 ms; field of view, 400.0 mm; and slice thickness, 6.0 mm.

In vivo chemo-photothermal therapy

For chemo-photothermal therapy, when the tumors grew to 5–6 mm in diameter, the mice were randomly divided into

eight groups (n=5 per group), namely PBS treated, PBS with NIR laser treated, Fe_3O_4@PDA-PEG NPs treated, Fe_3O_4@PDA-PEG NPs with NIR laser treated, Fe_3O_4@PDA-PEG-EGFR NPs treated, Fe_3O_4@PDA-PEG-EGFR NPs with NIR laser treated, Fe_3O_4@PDA-PEG-EGFR-DOX NPs treated, and Fe_3O_4@PDA-PEG-EGFR-DOX NPs with NIR laser treated. Mice of each group were intravenously injected with 100 μL of PBS, Fe_3O_4@PDA-PEG NPs, Fe_3O_4@PDA-PEG-EGFR NPs, or Fe_3O_4@PDA-PEG-EGFR-DOX NPs. The mice were anesthetized with chloral hydrate (5%), and the tumors were irradiated with or without an 808 nm laser (0.6 W/cm^2) for 6 min after 24 h injection. After treatments, the length and width of the tumors were tracked with a caliper every 2 days for 14 days. The tumor volume was calculated as follows: Tumor volume = (tumor length) × (tumor width)^2/2. The relative tumor growth ratio was calculated as V/V_0, where V and V_0 were the tumor volumes on day 14 and day 0, respectively.

Histological analysis

BALB/c mice from the treatment group were killed, and the tumor tissues and other major organs including heart, liver, spleen, lung, and kidney were collected for analysis after various treatments. The frozen tissue slides were further stained with hematoxylin and eosin following the standard protocol and examined using a fluorescence microscope.

Statistical analysis

All values are expressed as the mean ± SD and analyzed by using Student's *t*-test. *P*-values <0.05 were considered statistically significant.

Results and discussion

Preparation and characterization of Fe_3O_4@PDA-PEG-EGFR-DOX NPs

The Fe_3O_4@PDA-PEG-EGFR-DOX NPs were prepared as shown in Figure 1. Fe_3O_4@PDA NPs were synthesized through spontaneous in situ polymerization of PDA. After coating, the average size of Fe_3O_4@PDA NPs was determined by TEM and DLS. The average size of Fe_3O_4@PDA observed from TEM was ~60 nm (Figure 2A), whereas the average hydrodynamic diameter measured by DLS was ~91.2±31.1 nm (Figure 2B). Absorption bands, 3,421 cm^{-1} (N-H stretching) and 1,524 cm^{-1} (N-H bending) in the FT-IR spectrum of Fe_3O_4@PDA (as shown in Figure 2C) further confirmed the presence of PDA on Fe_3O_4. Then, the Fe_3O_4@PDA NPs thus obtained were sequentially modified with NH_2-PEG-COOH and EGFR antibody via covalent conjugation to form Fe_3O_4@PDA-PEG-EGFR NPs. The NH_2-PEG-COOH was conjugated onto the surface of Fe_3O_4@PDA NPs through the reaction between terminal amine group of NH_2-PEG-COOH and catechol group of PDA by a Schiff base reaction pathway. As illustrated in the FT-IR absorption spectrum (Figure 2C), the characteristic peaks of NH_2-PEG-COOH at 3,393 cm^{-1} (O-H stretching), 1,635 cm^{-1} (C=O stretching), and 1,109 cm^{-1} (C-O-C stretching) indicated that NH_2-PEG-COOH had been successfully conjugated onto the Fe_3O_4@PDA NPs. The EGFR antibody was successfully conjugated to Fe_3O_4@PDA-PEG NPs, which was proved by SDS-PAGE analysis. As shown in Figure 2D, the Coomassie blue-stained protein band represented the free EGFR antibody and Fe_3O_4@PDA-PEG-EGFR NPs that were diffused in gel. For Fe_3O_4@PDA-PEG-EGFR NPs, the Coomassie blue-stained EGFR antibody colocalized with Fe_3O_4@PDA-PEG NPs, indicating that EGFR antibody was chemically linked to the surface of the Fe_3O_4@PDA-PEG NPs. In contrast, Fe_3O_4@PDA-PEG NPs have no corresponding band by Coomassie blue-stained gel analysis. All of these results suggested that Fe_3O_4@PDA-PEG-EGFR NPs had been successfully constructed.

Because of the presence of magnetic iron oxide core, the Fe_3O_4@PDA-PEG-EGFR NPs displayed strong magnetic property. When placed beside a magnet, the Fe_3O_4@PDA-PEG-EGFR NPs in aqueous solution was attracted by a magnet, which was almost unchanged without a magnet (Figure 3A). The strong super paramagnetism of Fe_3O_4@PDA-PEG-EGFR NPs was further revealed by the field-dependent magnetization hysteresis loop (Figure 3B). Fe_3O_4 NPs have been widely used as a T_2-contrast agent for MRI.[24,25] As shown in Figure 3C and D, the T_2-weighted MR images exhibited increasingly darkening effect with the increase of Fe_3O_4@PDA-PEG-EGFR NPs concentration. This result suggested that Fe_3O_4@PDA-PEG-EGFR NPs could be used as a T_2-weighted MRI contrast agent.

Photothermal properties of Fe_3O_4@PDA-PEG-EGFR NPs

The photothermal conversion capability of Fe_3O_4@PDA-PEG-EGFR NPs was evaluated by irradiating Fe_3O_4@PDA-PEG-EGFR aqueous solution with an 808 nm NIR laser at 0.6 W/cm^2. As shown in Figure 4A, the temperature strikingly rised with increasing concentration of Fe_3O_4@PDA-PEG-EGFR NPs, following a time- and concentration-dependent manner. In particular, at an Fe_3O_4@PDA-PEG-EGFR NPs concentration of 150 μg/mL, the solution temperature could reach 50°C within 6 min irradiation, which is the temperature required to kill cancer cells.[26] The thermal stability of Fe_3O_4@PDA-PEG-EGFR NPs was assessed by NIR laser irradiations at 0.6 W/cm^2 for

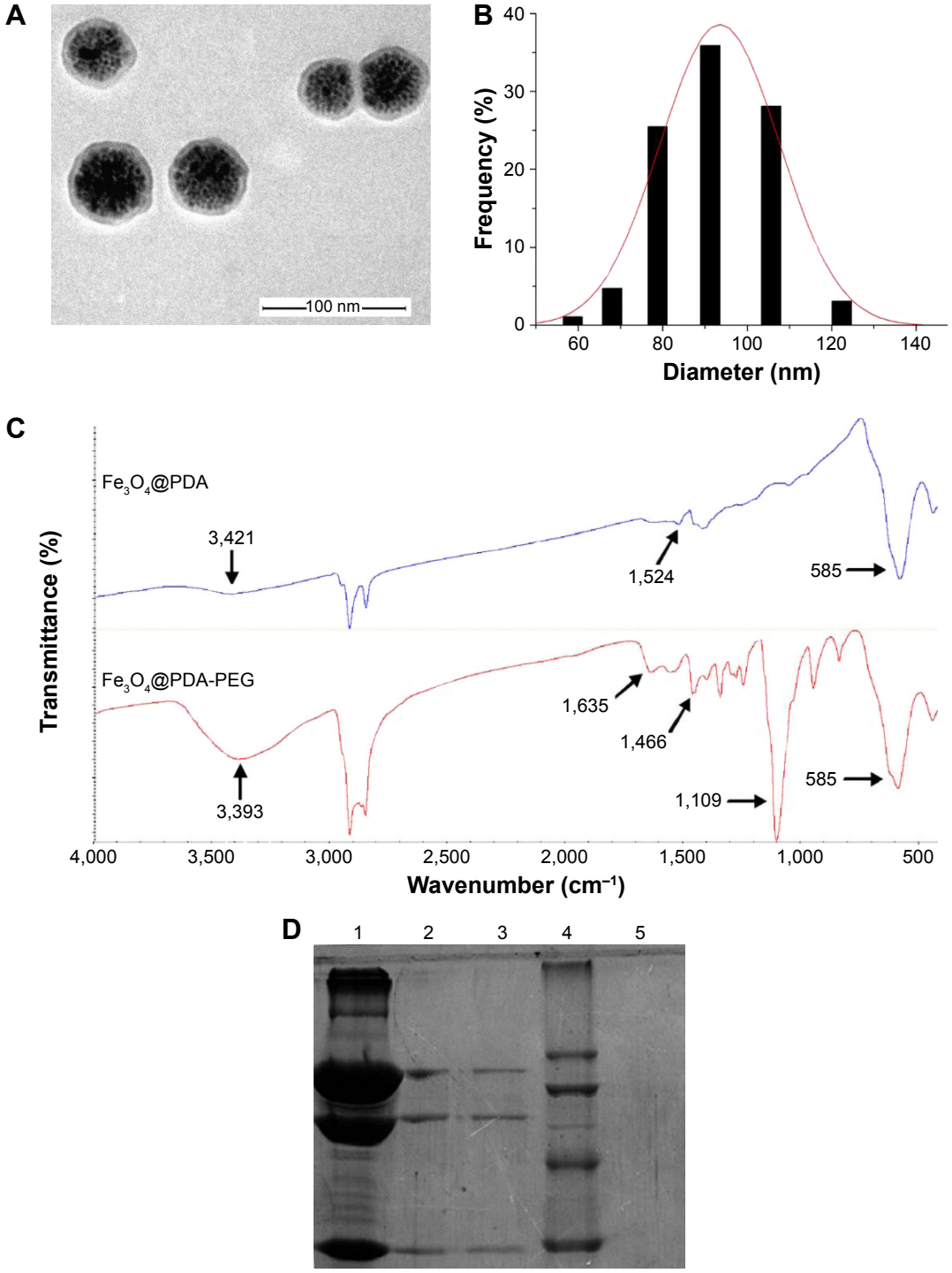

Figure 2 Confirmation of the bioconjugation of EGFR antibody to Fe_3O_4@PDA NPs.
Notes: (**A**) TEM image and (**B**) size distribution histogram of the Fe_3O_4@PDA NPs. (**C**) FT-IR spectra of Fe_3O_4@PDA and Fe_3O_4@PDA-PEG. (**D**) SDS-PAGE analysis of Fe_3O_4@PDA-PEG-EGFR and EGFR antibody. The Coomassie blue-stained gel analysis revealed the successful cross-linking of EGFR antibody molecules on the surface of the Fe_3O_4@PDA-PEG NPs. Lane 1, EGFR antibody; lanes 2 and 3, the bioconjugated Fe_3O_4@PDA-PEG-EGFR NPs; lane 4, protein molecular weight marker; lane 5, Fe_3O_4@PDA-PEG NPs.
Abbreviations: FT-IR, Fourier transform–infrared; SDS-PAGE, sodium dodecyl sulfate–polyacrylamide gel electrophoresis; TEM, transmission electron microscope; PDA, polydopamine; PEG, polyethylene glycol; NP, nanoparticle.

6 min, followed by natural cooling of temperature to room temperature for five cycles. After five cycles of laser irradiation, there was no noticeable attenuation in the thermal conversion efficiency of the Fe_3O_4@PDA-PEG-EGFR NPs (Figure 4B). The remarkable photothermal conversion efficiency and thermal stability indicated that the Fe_3O_4@PDA-PEG-EGFR NPs could be used as an excellent candidate for PTT applications.

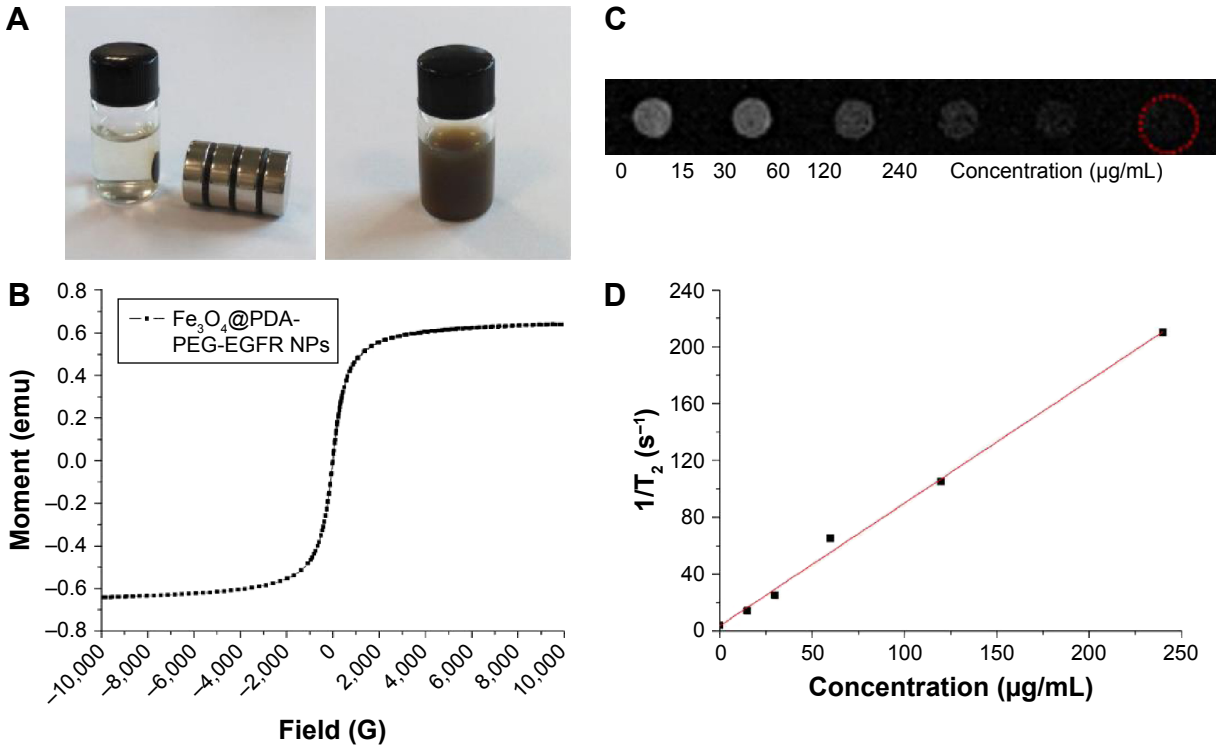

Figure 3 Magnetic properties of Fe_3O_4@PDA-PEG-EGFR NPs.
Notes: (**A**) Photographs of Fe_3O_4@PDA-PEG-EGFR in water with and without a magnet. (**B**) Magnetization loops of Fe_3O_4@PDA-PEG-EGFR NPs. (**C**) T_2-weighted MR images of Fe_3O_4@PDA-PEG-EGFR solutions at different concentrations. (**D**) T_2 relaxation rates (R_2) of Fe_3O_4@PDA-PEG-EGFR solutions at different concentrations.
Abbreviations: MR, magnetic resonance; PDA, polydopamine; PEG, polyethylene glycol; NP, nanoparticle.

Drug loading and releasing on Fe_3O_4@PDA-PEG-EGFR-DOX NPs

Chemotherapy drug DOX is mixed with Fe_3O_4@PDA-PEG-EGFR NPs in Tris-buffer (pH 8.0) overnight. As shown in Figure 5A, the UV-vis absorption spectrum of Fe_3O_4@PDA-PEG-EGFR-DOX NPs showed that the DOX characteristic peak shifted from 480 to ~500 nm, confirming the loading of DOX onto Fe_3O_4@PDA-PEG-EGFR NPs. The maximal DOX loading ratio (DOX:Fe_3O_4@PDA-PEG-EGFR NPs, w/w) was estimated to be ~80% (data not shown). Then, the drug-releasing capability of Fe_3O_4@PDA-PEG-EGFR-DOX NPs was examined at pH 5.0 and

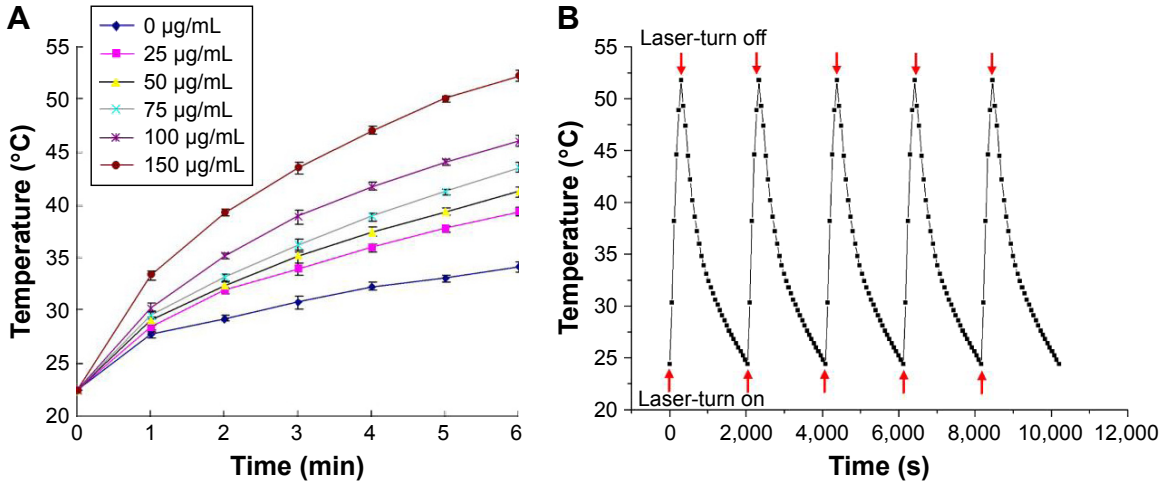

Figure 4 Photothermal properties of Fe_3O_4@PDA-PEG-EGFR NPs.
Notes: (**A**) Temperature elevation of Fe_3O_4@PDA-PEG-EGFR NP solution at various concentrations irradiated with an 808 nm NIR laser (0.6 W/cm^2, 6 min) measured every 1 min using a thermometer. (**B**) Temperature elevation of Fe_3O_4@PDA-PEG-EGFR NPs over five laser on/off cycles under NIR laser irradiation. Red arrows under the curve represent laser-turn on, red arrows on the curve represent laser-turn off.
Abbreviations: NIR, near-infrared; PDA, polydopamine; PEG, polyethylene glycol; NP, nanoparticle.

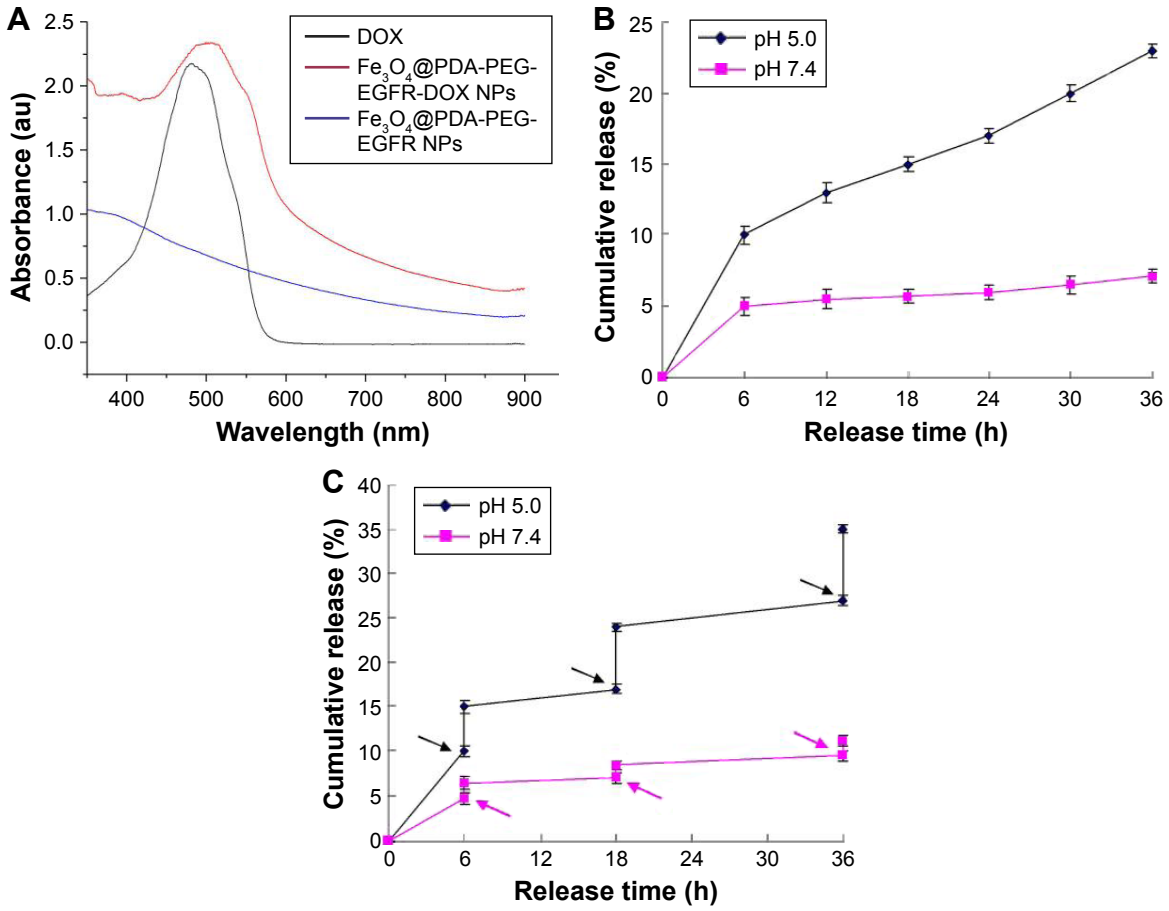

Figure 5 DOX loading and releasing.
Notes: (**A**) UV-vis absorbance spectra of DOX, Fe_3O_4@PDA-PEG-EGFR NPs, and Fe_3O_4@PDA-PEG-EGFR-DOX NPs. (**B**) DOX release from Fe_3O_4@PDA-PEG-EGFR NPs at different pH over 36 h. (**C**) NIR-triggered DOX release from Fe_3O_4@PDA-PEG-EGFR-DOX NPs. The samples at different pH were irradiated with an 808 nm NIR laser (0.6 W/cm^2) at different time points indicated by the arrows. Error bars mean standard deviations (n=3).
Abbreviations: DOX, doxorubicin; NIR, near-infrared; UV-vis, ultraviolet visible; PDA, polydopamine; PEG, polyethylene glycol; NP, nanoparticle.

7.4. As shown in Figure 5B, within 36 h, ~25% of DOX was released from the Fe_3O_4@PDA-PEG-EGFR-DOX NPs at pH 5.0 compared with 6% of DOX release at pH 7.4. The amount of DOX released from Fe_3O_4@PDA-PEG-EGFR-DOX NPs at pH 5.0 was approximately fourfold higher than that at pH 7.4. The protonation of the amino group in the DOX molecule gave DOX a positive charge and thus enhanced the hydrophilicity to trigger drug release at a lower pH.

To investigate the photothermal influence on DOX release, Fe_3O_4@PDA-PEG-EGFR-DOX NPs suspended in PBS at pH 5.0 or 7.4 were irradiated under an 808 nm NIR laser (0.6 W/cm^2, 6 min). As shown in Figure 5C, a significant thermo-triggered burst release of DOX from Fe_3O_4@PDA-PEG-EGFR-DOX NPs was observed at pH 5.0. In comparison, only limited DOX was released at pH 7.4 under the same condition. The pH-dependent NIR-triggered drug release processes enabled regulation of intracellular drug release and minimizing of the side effects of chemotherapy drugs.

Cellular uptake of Fe_3O_4@PDA-PEG-EGFR-DOX NPs

The cellular uptake and internalization of Fe_3O_4@PDA-PEG-EGFR-DOX NPs for the intracellular delivery of DOX were investigated by using DLD-1 human colon cancer cells. First, the level of EGFR expression on the surface of DLD-1 cells was detected by immunofluorescence (Figure 6A). The DLD-1 cells were incubated with Fe_3O_4@PDA-PEG-EGFR-DOX NPs for 6, 12, 24, and 36 h. With incubation time increasing from 6 to 36 h, the red fluorescence of DOX was gradually distributed in the cytoplasm and in the nuclei of the Fe_3O_4@PDA-PEG-EGFR-DOX NP-treated cells (Figure 6B). This result indicated that DOX molecules were released from Fe_3O_4@PDA-PEG-EGFR-DOX NPs taken up by DLD-1 cells. In addition, the DOX released from Fe_3O_4@PDA-PEG-EGFR-DOX NPs showed slow nuclear clustering because DOX was first released in the

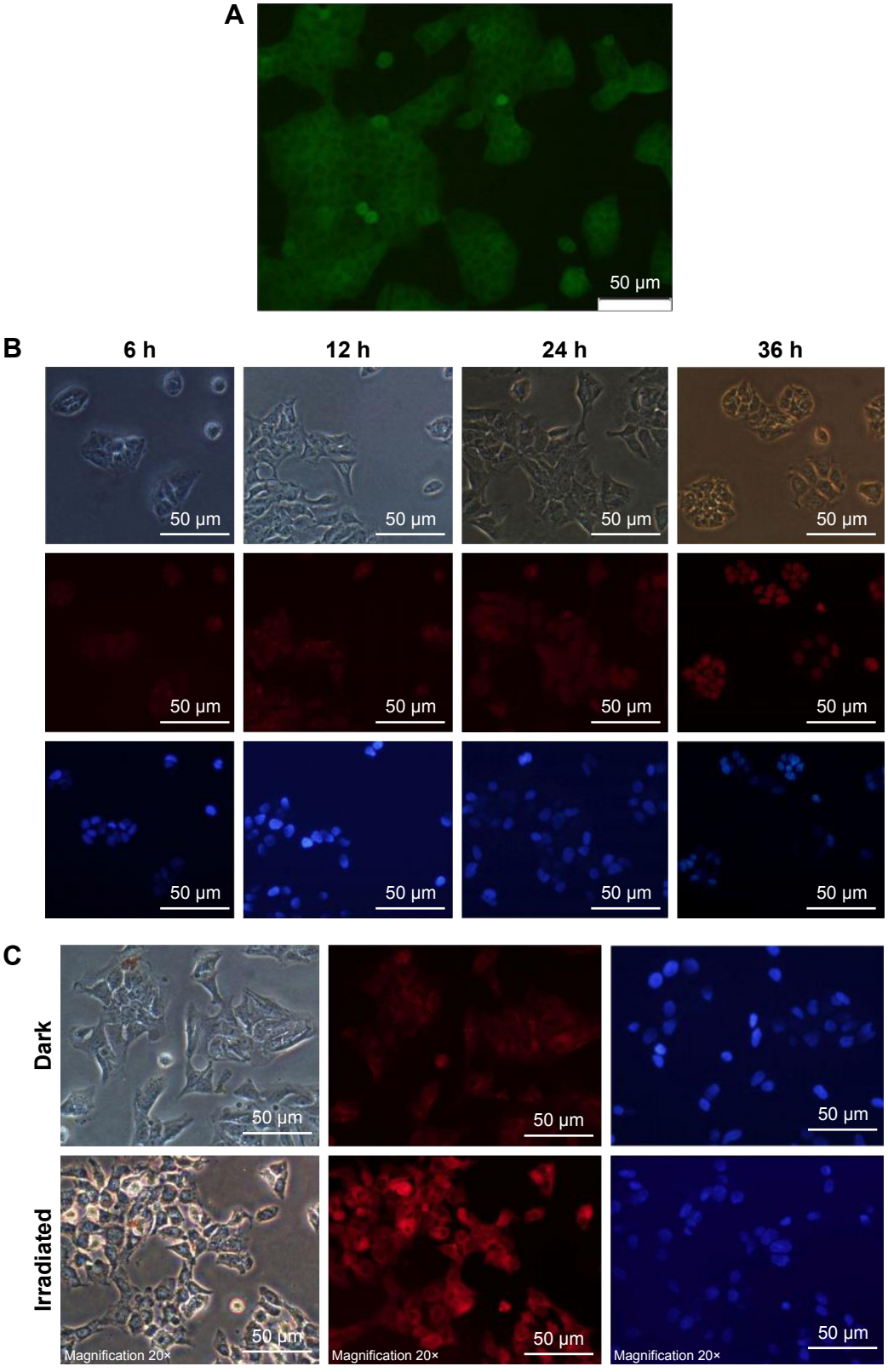

Figure 6 DOX release of Fe_3O_4@PDA-PEG-EGFR-DOX NPs under remote optical controls.
Notes: (**A**) The level of EGFR expression on the surface of DLD-1 cells was examined by immunofluorescence using an anti-EGFR antibody (green). Scale bar is 50 μm. (**B**) Fluorescence images of DLD-1 cells treated with Fe_3O_4@PDA-PEG-EGFR-DOX NPs for various times indicated. Images were taken from bright-field mode, DOX channel (red), and DAPI channel (blue), respectively. Scale bar is 50 μm. (**C**) Fluorescence images of DLD-1 cells incubated with Fe_3O_4@PDA-PEG-EGFR-DOX NPs with or without an 808 nm laser irradiation at 0.6 W/cm^2 for 6 min. Scale bar is 50 μm.
Abbreviations: DOX, doxorubicin; DAPI, 4,6-diamidino-2-phenylindole; PDA, polydopamine; PEG, polyethylene glycol; NP, nanoparticle.

cytoplasm, followed by entering into the nucleus. The cellular internalization of Fe_3O_4@PDA-PEG-EGFR-DOX NPs was consistent with other reported drug releasing systems.[7,27]

According to the previous studies, the mild photothermal heating caused by the NPs could not only trigger more release of DOX but also increase the cellular internalization of the NPs by promoting cellular metabolism and membrane permeability.[28–31] In order to further confirm whether the enhanced cell uptake of NPs could be triggered by laser irradiation, DLD-1 cells were incubated with Fe_3O_4@PDA-PEG-EGFR-DOX NPs and irradiated by an 808 nm NIR laser (0.6 W/cm^2) for 6 min. The fluorescence images displayed that the red fluorescence of DOX released from Fe_3O_4@PDA-PEG-EGFR-DOX NPs in DLD-1 cells was significantly enhanced after 6 min NIR irradiation in comparison with those without irradiation (Figure 6C). This result indicated that the intracellular release of DOX from internalized Fe_3O_4@PDA-PEG-EGFR-DOX NPs could be triggered by NIR irradiation.

Cell viability assay

A CCK-8 assay was employed to evaluate the viability of DLD-1 cells incubated with Fe_3O_4@PDA-PEG-EGFR NPs or Fe_3O_4@PDA-PEG-EGFR-DOX NPs at selected concentrations ranging from 0 to 100 μg/mL. As shown in Figure 7, >90% of DLD-1 cells remained viable after 24 h incubation with 100 μg/mL Fe_3O_4@PDA-PEG-EGFR NPs without an NIR laser exposure, confirming the negligible cytotoxicity of Fe_3O_4@PDA-PEG-EGFR NPs. In contrast, the cell viabilities were sharply decreased when DLD-1 cells were incubated with Fe_3O_4@PDA-PEG-EGFR NPs in the presence of an 808 nm NIR laser irradiation (0.6 W/cm^2) for 6 min (only 30% of remaining cell viability). Moreover, compared with Fe_3O_4@PDA-PEG-EGFR NPs, the inhibition effect of Fe_3O_4@PDA-PEG-EGFR-DOX NPs at an equivalent concentration appeared much stronger whether or not with NIR laser irradiation. These results suggested that Fe_3O_4@PDA-PEG-EGFR-DOX NPs had a prominent chemo-photothermal antitumor effect.

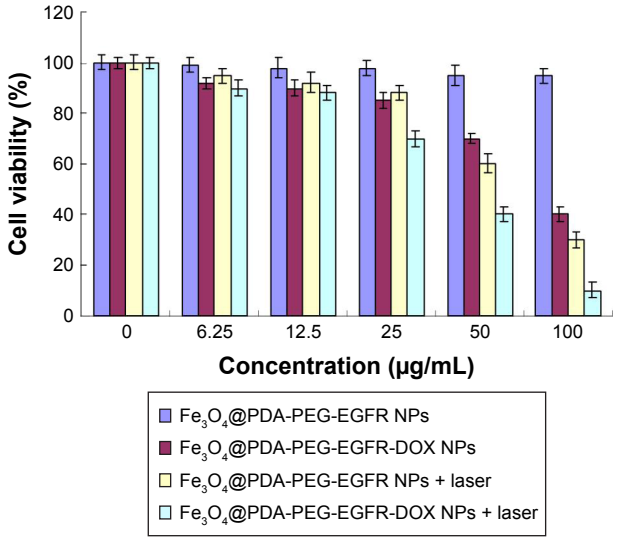

Figure 7 Effects of Fe_3O_4@PDA-PEG-EGFR-DOX NPs on cell viability in vitro.
Note: Viability of DLD-1 cells incubated with various concentrations of Fe_3O_4@PDA-PEG-EGFR NPs and Fe_3O_4@PDA-PEG-EGFR-DOX NPs with or without an 808 nm NIR laser irradiation at 0.6 W/cm^2.
Abbreviations: DOX, doxorubicin; NIR, near-infrared; PDA, polydopamine; PEG, polyethylene glycol; NP, nanoparticle.

In vivo targeting MRI of tumors

The excellent in vitro MRI contrast performance of Fe_3O_4@PDA-PEG-EGFR NPs inspired us to study their applicability in vivo. Mice bearing DLD-1 tumors were intravenously injected with Fe_3O_4@PDA-PEG-EGFR NPs (200 μL, 100 μg/mL) and imaged by a 3.0-T clinical MR scanner at 0, 12, and 24 h. A strong darkening effect in the tumor area was observed in T_2-weighted MR images at 24 h after injection (Figure 8), suggesting that Fe_3O_4@PDA-PEG-EGFR NPs could be used for MRI-guided cancer therapy.

Chemo-photothermal therapy

Because of the prominent antitumor effect in vitro, the inhibiting tumor effect of Fe_3O_4@PDA-PEG-EGFR-DOX NPs was evaluated in vivo. The mice were divided into eight randomized groups and were first treated through intravenous injection of different materials. After treatment, the tumor sizes in different groups of mice were measured every 2 days for a period of 14 days. As shown in Figure 9A and B, tumors in control groups, including PBS injection with or without laser irradiation, as well as Fe_3O_4@PDA-PEG injection without laser irradiation, all showed obvious growth. The growth of tumors was slightly increased by Fe_3O_4@PDA-PEG-EGFR-DOX NPs without laser irradiation, which is consistent with the previous reports that DOX at such a low dose could not effectively suppress tumor growth.[32] Importantly, more obvious tumor inhibiting effect was achieved from the group with Fe_3O_4@PDA-PEG-EGFR-DOX NPs injection and NIR laser irradiation during the 14 days. These in vivo results strongly demonstrated that Fe_3O_4@PDA-PEG-EGFR-DOX NPs were more efficient than monotherapy alone for ablation of tumors.

The potential toxicity of the NPs had been a major drawback for practical applications in vivo. In this experiment, it was found that mice in all test groups, especially for groups treated with Fe_3O_4@PDA-PEG-EGFR-DOX

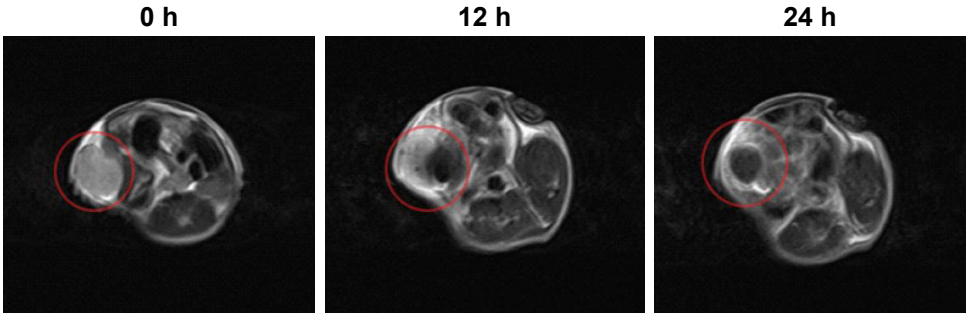

Figure 8 In vivo T_2-weighted MR images.
Notes: T_2-weighted MR images of mice after intravenous injection with Fe_3O_4@PDA-PEG-EGFR NPs at 0, 12, and 24 h. Red circle indicates tumor position.
Abbreviations: MR, magnetic resonance; PDA, polydopamine; PEG, polyethylene glycol; NP, nanoparticle.

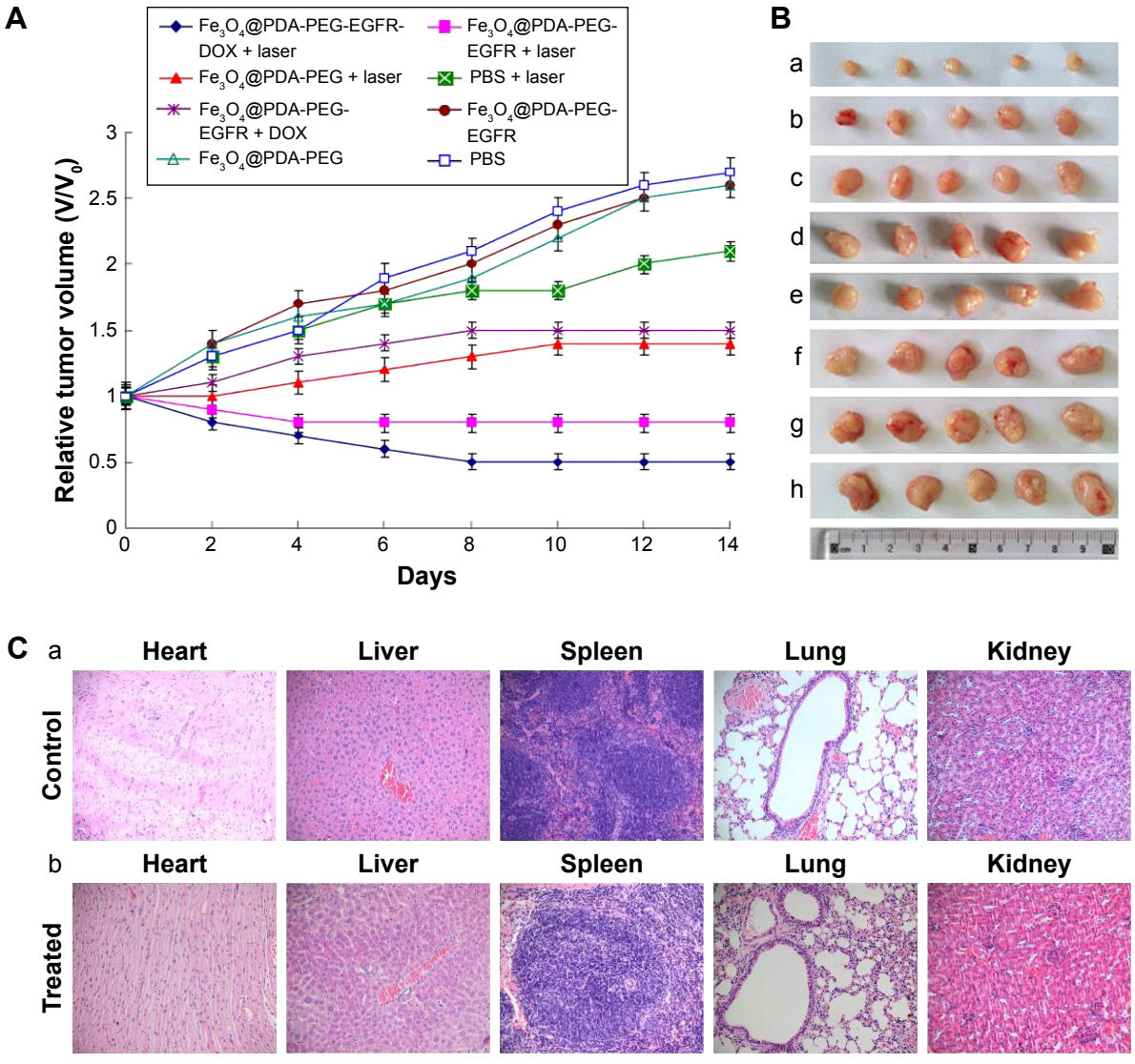

Figure 9 In vivo evaluation of chemo-photothermal therapeutic effect.
Notes: (**A**) Tumor growth curves of different groups of mice after treatment (day 14). The tumor volumes were normalized to their initial sizes. (**B**) Photographs of the tumors collected from different groups of mice after 14 days of treatment with (a) Fe_3O_4@PDA-PEG-EGFR-DOX + laser, (b) Fe_3O_4@PDA-PEG-EGFR + laser, (c) Fe_3O_4@PDA-PEG + laser, (d) PBS + laser, (e) Fe_3O_4@PDA-PEG-EGFR-DOX, (f) Fe_3O_4@PDA-PEG-EGFR, (g) Fe_3O_4@PDA-PEG, and (h) PBS. (**C**) Histology analysis of the major organs of mice after 30 days of treatment, from the different groups: (a) PBS group and (b) Fe_3O_4@PDA-PEG-EGFR-DOX irradiation with an 808 nm laser at 0.6 W/cm^2.
Abbreviations: PBS, phosphate-buffered saline; PDA, polydopamine; PEG, polyethylene glycol; NP, nanoparticle; DOX, doxorubicin.

NPs and NIR laser irradiation, behaved normally without a significant decrease in body weight (data not shown). The maintained body weight demonstrated that there was no noticeable toxicity of the prepared NPs in vivo. In addition, histological analysis of the major organs showed that there was no obvious tissue damage after 30 days of chemo-photothermal therapy, further confirming the low toxicity of the NPs in vivo (Figure 9C).

Conclusion

In summary, the multifunctional Fe_3O_4@PDA-PEG-EGFR-DOX NPs capable of simultaneous chemo-photothermal therapy and MRI have been successfully designed and synthesized. DOX could be physically adsorbed on Fe_3O_4@PDA-PEG-EGFR NPs with high drug-loading ratios via π–π stacking. The resultant NPs exhibited pH and heat-responsive DOX release. When the NPs were uptaken into the DLD-1 cells, the release of the DOX could be prompted by the NIR irradiation. Meanwhile, the cells were killed by the released DOX and the local heating under the NIR irradiation. The tumor growth was effectively inhibited by enhanced DOX release of the Fe_3O_4@PDA-PEG-EGFR-DOX NPs under the NIR irradiation and the NIR-induced PTT. The results of this study demonstrated that Fe_3O_4@PDA-PEG-EGFR-DOX NPs possessed sensitive drug release and prominent chemo-photothermal synergistic therapy effects for tumor inhibition and eradication.

Precision medicine is altering the traditional treatment methods for patients with cancer. Therefore, EGFR antibody-targeted Fe_3O_4@PDA-PEG-EGFR-DOX theranostic NPs are a promising receptor-targeted drug delivery system for the individual treatment of EGFR-overexpressed colon cancer.

Acknowledgments

This work was supported by grants from National Natural Science Foundation of China (No 31540082) and Microscale Chemistry for Medical Diagnosis and Treatment of Jilin University (No 419020201055).

Disclosure

The authors report no conflicts of interest in this work.

References

1. Maksimenko A, Dosio F, Mougin J, et al. A unique squalenoylated and nonpegylated doxorubicin nanomedicine with systemic long-circulating properties and anticancer activity. *Proc Natl Acad Sci U S A*. 2014;111(2):E217–E226.
2. Duncan R. Polymer conjugates as anticancer nanomedicines. *Nat Rev Cancer*. 2006;6(9):688–701.
3. Huang HC, Barua S, Sharma G, Dey SK, Rege K. Inorganic nanoparticles for cancer imaging and therapy. *J Control Release*. 2011;155(3):344–357.
4. Sundstrom T, Daphu I, Wendelbo I, et al. Automated tracking of nanoparticle-labeled melanoma cells improves the predictive power of a brain metastasis model. *Cancer Res*. 2013;73(8):2445–2456.
5. Parsian M, Unsoy G, Mutlu P, Yalcin S, Tezcaner A, Gunduz U. Loading of gemcitabine on chitosan magnetic nanoparticles increases the anticancer efficacy of the drug. *Eur J Pharmacol*. 2016;784:121–128.
6. Quinto CA, Mohindra P, Tong S, Bao G. Multifunctional superparamagnetic iron oxide nanoparticles for combined chemotherapy and hyperthermia cancer treatment. *Nanoscale*. 2015;7(29):12728–12736.
7. Peng M, Li H, Luo Z, et al. Dextran-coated superparamagnetic nanoparticles as potential cancer drug carriers in vivo. *Nanoscale*. 2015;7(25):11155–11162.
8. Liu Y, Ai K, Lu L. Polydopamine and its derivative materials: synthesis and promising applications in energy, environmental, and biomedical fields. *Chem Rev*. 2014;114(9):5057–5115.
9. Lee H, Dellatore SM, Miller WM, Messersmith PB. Mussel-inspired surface chemistry for multifunctional coatings. *Science*. 2007;318(5849):426–430.
10. Liu X, Cao J, Li H, et al. Mussel-inspired polydopamine: a biocompatible and ultrastable coating for nanoparticles in vivo. *ACS Nano*. 2013;7(10):9384–9395.
11. Jori G, Spikes JD. Photothermal sensitizers: possible use in tumor therapy. *J Photochem Photobiol B*. 1990;6(1–2):93–101.
12. Hirsch LR, Stafford R, Bankson J, et al. Nanoshell-mediated near-infrared thermal therapy of tumors under magnetic resonance guidance. *Proc Natl Acad Sci U S A*. 2003;100(23):13549–13554.
13. Liu Y, Ai K, Liu J, Deng M, He Y, Lu L. Dopamine-melanin colloidal nanospheres: an efficient near-infrared photo-thermal therapeutic agent for in vivo cancer therapy. *Adv Mater*. 2013;25(9):1353–1359.
14. Lin LS, Cong ZX, Cao JB, et al. Multifunctional Fe_3O_4@polydopamine core-shell nanocomposites for intracellular mRNA detection and imaging-guided photothermal therapy. *ACS Nano*. 2014;8(4):3876–3883.
15. Martín M, Salazar P, Villalonga R, Campuzano S, Pinagarrón JM, González-Mora JL. Preparation of core-shell Fe_3O_4@poly(dopamine) magnetic nanoparticles for biosensor construction. *J Mater Chem B*. 2014;2:739–746.
16. Zha Z, Zhang S, Deng Z, et al. Enzyme responsive copper sulphide nanoparticles for combined photoacoustic imaging, tumor-selective chemotherapy and photothermal therapy. *Chem Commun*. 2013;49(33):3455–3457.
17. You J, Zhang G, Li C. Exceptionally high payload of doxorubicin in hollow Gold nanospheres for near-infrared light-triggered drug release. *ACS Nano*. 2010;4(2):1033–1041.
18. Shen P, Hawksworth J, Lovato J, Li Y, Li C, Dai Z. Cytoreductive surgery and intraperitoneal hyperthermic chemotherapy with mitomycin C for peritoneal carcinomatosis from nonappendiceal colorectal carcinoma. *Ann Surg Oncol*. 2004;11(2):178–186.
19. Huebsch N, Mooney DJ. Inspiration and application in the evolution of biomaterials. *Nature*. 2009;462(7272):426–432.
20. Davis ME, Shin DM. Nanoparticle therapeutics: an emerging treatment modality for cancer. *Nat Rev Drug Discov*. 2008;7(9):771–782.
21. Xuan SH, Wang F, Wang Y, Yu JC, Leung KCF. Facile synthesis of size-controllable monodispersed ferrite nanospheres. *J Mater Chem*. 2010;20(24):5086–5094.
22. Liu FY, He XX, Lei Z, et al. Facile preparation of doxorubicin-loaded upconversion@polydopamine nanoplatforms for simultaneous in vivo multimodality imaging and chemophotothermal synergistic therapy. *Adv Healthc Mater*. 2015;4(4):559–568.
23. Laemmli UK. Cleavage of structural proteins during assembly of the head of bacteriophage T4. *Nature*. 1970;277(5259):680–685.
24. Shi X, Gong H, Li Y, Wang C, Cheng L, Liu Z. Graphene-based magnetic plasmonic nanocomposite for dual bioimaging and photothermal therapy. *Biomaterials*. 2013;34(20):4786–4793.

25. Girard OM, Ramirez R, McCarty S, Mattrey RF. Toward absolute quantification of iron oxide nanoparticles as well as cell internalized fraction using multiparametric MRI. *Contrast Media Mol Imaging*. 2012;7:411–417.
26. Habash RWY, Bansal R, Krewski D, Alhafid HT. Thermal therapy, part 1: an introduction to thermal therapy. *Crit Rev Biomed Eng*. 2006; 34(6):459–489.
27. Wang C, Cheng L, Liu Z. Drug delivery with upconversion nanoparticles for multi-functional targeted cancer cell imaging and therapy. *Biomaterials*. 2011;32(4):1110–1120.
28. Wang C, Xu H, Liang C, et al. Iron oxide@polypyrrole nanoparticles as a multifunctional drug carrier for remotely controlled cancer therapy with synergistic antitumor effect. *ACS Nano*. 2013;7(8):6782–6795.
29. Zhang Z, Wang J, Chen C. Near-infrared light-mediated nanoplatforms for cancer thermo-chemotherapy and optical imaging. *Adv Mater*. 2013; 25(28):3869–3880.
30. Sherlock SP, Tabakman SM, Xie LM, Dai HJ. Photothermally enhanced drug delivery by ultrasmall multifunctional FeCo/graphitic shell nanocrystals. *ACS Nano*. 2011;5(2):1505–1512.
31. Feng L, Yang X, Shi X, et al. Polyethylene glycol and polyethylenimine dual-functionalized nanographene oxide for photothermally enhanced gene delivery. *Small*. 2013;9(11):1989–1997.
32. Liu T, Wang C, Gu X, et al. Drug delivery with PEGylated MoS_2 nano-sheets for combined photothermal and chemotherapy of cancer. *Adv Mater*. 2014;26(21):3433–3440.